IEEE Access
Multidisciplinary ⋮ Rapid Review ⋮ Open Access Journal

Received August 27, 2019, accepted September 10, 2019, date of publication September 16, 2019, date of current version September 27, 2019.

Digital Object Identifier 10.1109/ACCESS.2019.2941652

A Switching Hybrid LCC-S Compensation Topology for Constant Current/Voltage EV Wireless Charging

YAFEI CHEN, (Student Member, IEEE), HAILONG ZHANG, (Student Member, IEEE), SUNG-JUN PARK, AND DONG-HEE KIM, (Member, IEEE)
Department of Electrical Engineering, Chonnam National University, Gwangju 61186, South Korea

Corresponding author: Dong-Hee Kim (kimdonghee@jnu.ac.kr)

This work was supported in part by the National Research Foundation of Korea (NRF) Grant funded by the Korea Government (MSIT) under Grant NRF-2017R1C1B2010057.

ABSTRACT Wireless power transfer (WPT) technology has been widely applied to automobile industries, household electronics and medical devices because of its many advantages. The hybrid battery charging scheme, which combines constant voltage (CV) and constant current (CC), is considered to be quite reasonable in view of the limitations of the conventional CC/CV implementation scheme. In this study, based on the inductance and double capacitances-series (LCC-S) compensation topology, a switching hybrid topology is proposed for CC/CV electric vehicle (EV) battery charging. The topology parameters are designed according to the specified CV and zero phase angle (ZPA). In the CC charging mode, two additional capacitances are added to the topology for CC and ZPA implementation. Based on the proposed weak communication, the CC and CV charging mode can be converted via two AC switches (ACSs). The proposed hybrid system provides a simple structure, easy controllability, and stable output. A 2.5-kW experimental prototype is configured to verify the proposed hybrid charger. The maximum DC efficiencies (at 2.5-kW) of the CC and CV charging modes are 89.28% and 88.33%, respectively.

INDEX TERMS Wireless power transfer (WPT), electric vehicle (EV), switching hybrid topology, inductance and double capacitances-series (LCC-S), constant current/constant voltage (CC/CV).

I. INTRODUCTION

Electric vehicle (EV) battery charging methods involve both contact charging and wireless charging [1]–[3]. To achieve power transfer, contact charging utilizes the metal contact between the plug and the socket, while wireless charging utilizes the electromagnetic field [4]. Compared with contact charging, wireless charging has the advantages of no contact loss, no mechanical wear, safety, and reliability [5], [6]. Thus, wireless charging has received increasing attention.

Several EV battery charging strategies exist, such as CC charging, CV charging, and CC/CV hybrid charging [7]. In the CC charging process, the charging current is constant and independent of load variations. CC charging can implement fast charging; however, overvoltage is easily induced and can damage batteries. In the CV charging process, the charging voltage is a constant and independent of load variations; it rarely causes overvoltage, but it often induces insufficient charging and hampers the charging effect. The advantages of CC and CV charging can be combined based on the characteristics of a battery. Generally, CC/CV hybrid charging is widely utilized in the EV industry [8], [9]. The typical profile of CC/CV hybrid charging is shown in Fig. 1. The entire charging process is divided into two stages: CC mode and CV mode [10]. In CC mode, the charging current is constant while the charging voltage gradually increases. The CV mode begins when the charging voltage increases to a specified voltage, at which it remains constant, and the charging current slowly decreases to zero. The equivalent resistance continues to rise throughout the charging process.

In a wireless power transfer (WPT) system, there are generally two factors that should be considered simultaneously: zero voltage switching (ZVS) operations are required to reduce electromagnetic interference (EMI) and improve

The associate editor coordinating the review of this manuscript and approving it for publication was Sze Sing Lee.

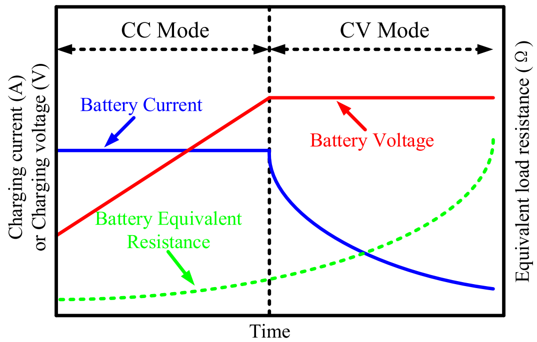

FIGURE 1. Typical profile of EV battery charging.

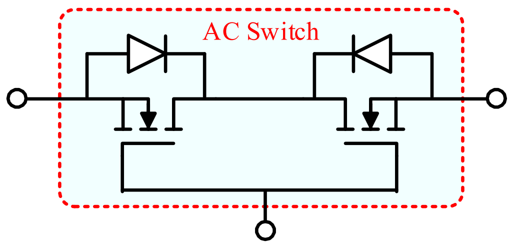

FIGURE 2. Structure diagram of MOSFET-type AC switch (ACS).

the transfer efficiency [11], and CC/CV hybrid charging is required to ensure long life span and maximum capacity utilization of batteries [12]. Currently, three primary schemes are utilized to achieve these factors. In the first [13]–[15], a few additional DC/DC converters are added behind the secondary side rectifier to implement post regulation. Impedance matching and CC/CV output can be obtained via duty cycle adjustment. However, the additional DC/DC converters result in low system efficiency and high cost. The second involves combining the frequency modulation (FM) control, phase-shift (PS) control, and other advanced controls to achieve ZVS operation and CC/CV output. In [16], a hybrid control approach is proposed within a limited operating frequency range. FM control is applied to achieve ZVS operation and PS control is applied to regulate the output voltage, respectively. In [17], a self-oscillating control method is proposed. According to the charging profile, the operation frequency of series-series (SS) compensation topology can be automatically adjusted between CC and CV operation points. These two control schemes can ensure ZVS operations and output regulations without the need for additional hardware devices. However, a wide FM range is generally required, which may increase the switching loss and VA rating. In addition, these control schemes are complex and require high speed real-time communication between the transmitter and receiver. The third scheme involves the reconfiguration of the compensation topologies using AC switches (ACSs). The typical structure of an ACS is shown in Fig. 2.

In fact, the common compensation topologies can be seen as combinations of a passive resonant network [18]. These networks have CC or CV output characteristics; integrating these networks and switching the states using ACSs can achieve ZVS and CC/CV output simultaneously. Because this scheme provides easy controllability and low cost, it is widely studied and applied today. In [19], a composite topology, which is a combined SS and series-parallel (SP), is proposed. CC/CV output can be realized by switching; however, because a center-tapped transformer and three ACSs are required, the topology is complex. In [20], two composite topologies with CC/CV output via switching between the four basic composition topologies (SS, SP, parallel-series (PS) and parallel- parallel (PP)) is proposed. Nevertheless, the four conventional topologies are more sensitive to the load variations and have low parametric degrees of freedom. In addition, three ACSs are also utilized to switch the operation modes. In [21], a hybrid topology with two ACSs and an auxiliary capacitor at receiver side is proposed to achieve the required CC or CV charging. Unfortunately, the proposed hybrid topology for CC mode can be considered as an equivalent S-S compensation topology, the problems similar with in [20] also exist. In [22], a hybrid topology is proposed by using a single Full-bridge inverter (FBI) to implement CC/CV charging for massive electric bicycles (EBs). Configurable CC and CV outputs can be realized by turning on/off two ACSs. However, massive resonant devices are required to constitute the hybrid topology. In [23], a hybrid and reconfigurable IPT system with 3-D misalignment tolerance for CC and CV outputs is proposed. However, the utilized 4-coils structure with mutual inductances increases the complexity and cost. Furthermore, most of the proposed hybrid topologies are researched and applied to low power WPT applications (less than 1-kW), the relevant researches for EV application is still less.

In practical WPT applications, conventional control methods, e.g., FM control, PS control, and zero phase angle (ZPA) automatic tracking control usually require high-speed and real-time feedback of information (battery voltage/current, state of charge (SOC), etc.) from the receiver to the transmitter via wireless communication (Zigbee, Wi-Fi, Bluetooth, etc.) [24], [25]. Since the specifics of WPT applications, the applications of the general wireless communications in wireless charging result in disadvantages such as the susceptibility to disturbance, easy disconnection and data delay [26]–[28]. However, in the WPT system based on the switching hybrid topology, a concept of weak communication is proposed here, because the CC/CV charging can be implemented without continuous feedback from the secondary to the primary side. Weak communication does not represent a lack of communication between the transmitter and receiver, but the communication consists of only a charging start/stop signal, CC/CV mode conversion signal, and a few other discrete signals. Thus, the communication complexity reduces and fault tolerance increases because of the weak communication.

In this study, in order to achieve CC and CV charging characteristics, a switching hybrid topology based on LCC-S is proposed. The characteristics of the proposed topology are analyzed via the transformer T model. The conditions of constant output and ZPA in the CV and CC modes,

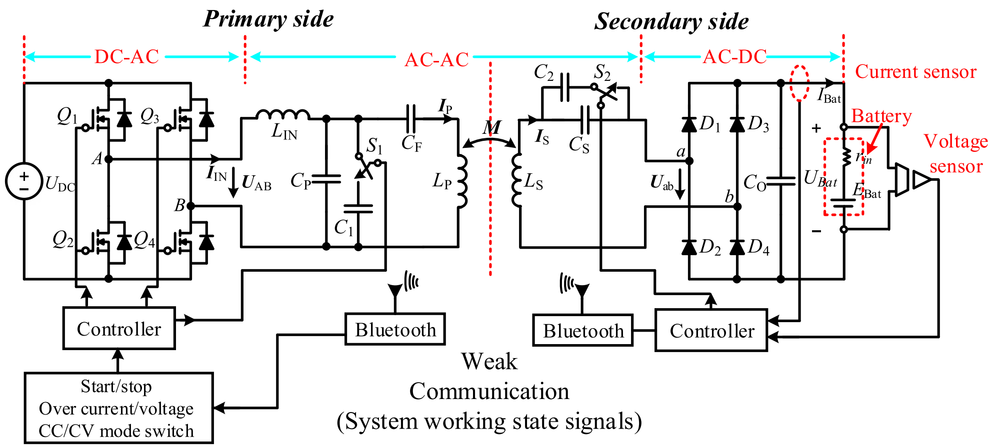

FIGURE 3. Proposed switching hybrid LCC-S WPT system with weak communication.

respectively, are given. The topology parameters of the CV charging mode are designed according to the specified charging voltage and ZPA requirements. In the CC charging mode, on the premise that this does not affect the other parameters, two additional capacitances are added to the topology via two ACSs: the additional primary capacitance for CC output and the additional assistant capacitance for ZPA. Based on the weak communication, the control scheme of the proposed hybrid charger is introduced. Finally, a 2.5-kW experimental prototype is configured, and comparative experiments are conducted to verify the proposed hybrid charger.

II. THEORETICAL ANALYSIS

Fig. 3 shows the structure of the proposed switching hybrid LCC-S WPT system with weak communication. U_{DC} is the DC-link voltage, which is normally produced by an active three-phase rectifier (ATPR) [29]. Q_1–Q_4 are four metallic oxide semiconductor field effect transistors (MOSFETs) that construct the FBI to convert the DC component into an AC component. $\boldsymbol{U}_{AB}$ and $\boldsymbol{I}_{IN}$ are the output voltage and current, respectively, of the FBI. If $\boldsymbol{U}_{AB}$ is expanded by the Fourier series, it can be expressed as

$$\mathbf{U}_{AB} = \frac{4U_{DC}}{\pi} \sum_{n=1,3,5...} \frac{\sin(n\varphi)}{n} \tag{1}$$

where n is the number of harmonics and φ is the phase angle. Generally, since the quality factors of the compensation topologies in WPT system are quite high, the current components of $\boldsymbol{I}_{IN}$ corresponding to the ultraharmonics are very small. Thus, the fundamental harmonic analysis (FHA) can be utilized without compromising on accuracy [14]. When only the fundamental component is considered, there is $n = 1$. In the LCC-S resonant network shown in Fig. 3, C_1 and C_2 are two additional capacitors to implement CC/CV output, and S_1 and S_2 are the corresponding ACSs to switch the charging modes. The specific working principles as well as switching guidelines will be introduced in detail in subsequent sections. The bridge rectifier (BR) on the secondary side consists of four diodes D_1–D_4. The BR is applied to transform the AC output voltage $\boldsymbol{U}_{ab}$ and current $\boldsymbol{I}_S$ to battery charging voltage U_{Bat} and current I_{Bat}, respectively. Since the output low-pass filter (LPF) consists only of the capacitance C_O, the following equations can be derived according to [30]:

$$U_{Bat} = \frac{\pi\sqrt{2}}{4} U_{ab} \tag{2}$$

$$I_{Bat} = \frac{2\sqrt{2}}{\pi} I_S \tag{3}$$

where U_{ab} and I_S are the RMS values of $\boldsymbol{U}_{ab}$ and $\boldsymbol{I}_S$, respectively. The output AC equivalent resistance is defined as $R_{Ac} = U_{ab}/I_S$, and the equivalent battery resistance is $R_{Bat} = U_{Bat} / I_{Bat}$. According to (2) and (3), the relational expression between R_{Ac} and R_{Bat} can be obtained by

$$R_{Ac} = \frac{8}{\pi^2} R_{Bat} \tag{4}$$

In a WPT system, the loosely coupled transformer (LCT) is a key component that affects the efficiency and output characteristics of the system [31]. Generally, two analytical models called the M and T models are used to analyze the LCT, as shown in Fig. 4. In order to simplify the analysis, the parasitic coil resistances are omitted. L_P andL_S are the self-inductances of the primary and secondary coils, respectively. M is the mutual inductance of the LCT, $\boldsymbol{U}_P$ and $\boldsymbol{U}_S$ are the coil voltages, and $\boldsymbol{I}_P$ and $\boldsymbol{I}_S$ are the coil currents. By Kirchhoff's voltage law (KVL), the following equations can be obtained from Fig. 4(a):

$$\begin{cases} \mathbf{U}_P = j\omega L_P \mathbf{I}_P - j\omega M \mathbf{I}_S \\ \mathbf{U}_S = j\omega M \mathbf{I}_P + j\omega L_S \mathbf{I}_S \end{cases} \tag{5}$$

on the premise that the M and T models are equivalent; the following equations can be derived by solving (5):

$$\begin{cases} L_T = L_P - M \\ L_R = L_S - M \end{cases} \tag{6}$$

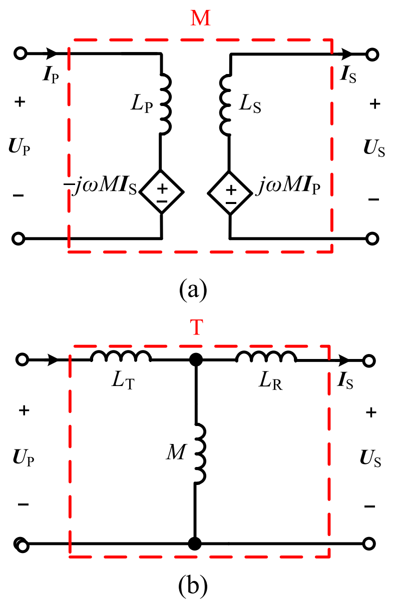

FIGURE 4. **Equivalent models of loosely coupled transformer. (a) M model; (b) T model.**

where L_T and L_R are the leakage inductances of the primary and secondary coils, respectively, when the turn ratio is same.

Fig. 5 shows three of types of the several passive resonant networks with CV or CC output that are possible in a WPT system. In these passive resonant networks, the relevance of the CV or CC output characteristics to the load impedance Z is dependent on the type of AC power source, i.e., an AC voltage source (ACVS) or an AC current source (ACCS) must be applied to the specific resonant network. In Fig. 5(a), when L resonates with C, i.e.,

$$\omega^2 = \frac{1}{LC} \tag{7}$$

where ω is the operating frequency of AC power source. On the basis of KVL and Kirchhoff's current law (KCL), the passive resonant network output current $\boldsymbol{I}_{V-C}$ in the resonant state can be derived as

$$\mathbf{I}_{V-C} = -j\,\mathbf{U}_{IN}\sqrt{\frac{C}{L}} = -j\frac{\mathbf{U}_{IN}}{\omega L} \tag{8}$$

According to (8), if the RMS value of $\boldsymbol{U}_{IN}$ is constant, the RMS value of $\boldsymbol{I}_{V-C}$ is constant as well, and $\boldsymbol{I}_{V-C}$ is independent of Z.

The C-V type passive resonant network shown in Fig. 5(b) has a similar analytical process when the operating angular frequency ω satisfies (7), i.e., L resonates with C. According to KVL and KCL, the output voltage $\boldsymbol{U}_{C-V}$ of C-V type network in the resonant state can be given as

$$\mathbf{U}_{C-V} = j\mathbf{I}_{IN}\sqrt{\frac{L}{C}} = j\omega L\mathbf{I}_{IN} \tag{9}$$

Similarly, if the RMS value of $\boldsymbol{I}_{IN}$ is constant, the RMS value of $\boldsymbol{U}_{V-C}$ is constant as well, and $\boldsymbol{U}_{V-C}$ is independent of Z.

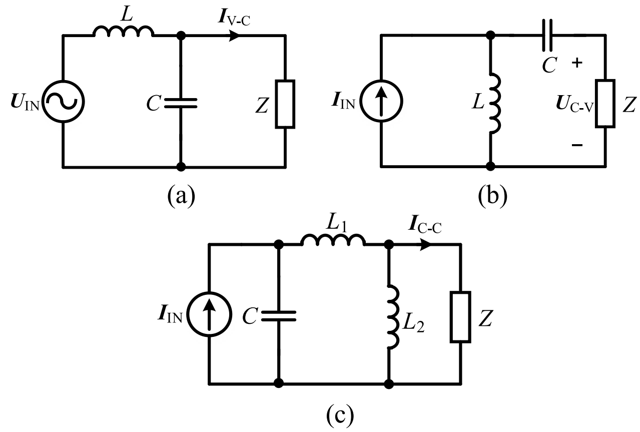

FIGURE 5. **Resonant network configuration with CV or CC output. (a) V-C type; (b) C-V type; (c) C-C type.**

The C-C type passive resonant network shown in Fig. 5(c) is a π-circuit, defined by $Z_C = 1 / j\omega C$, $Z_1 = j\omega L_1$ and $Z_2 = j\omega L_2$. Thus, on the basis of KVL and KCL, the relational expression between $\boldsymbol{I}_{IN}$ and $\boldsymbol{I}_{C-C}$ can be expressed as

$$\begin{aligned}\boldsymbol{I}_{IN} &= \frac{ZZ_2 + (Z+Z_2)(Z_C+Z_1)}{Z_2 Z_C}\boldsymbol{I}_{C-C} \\ &= \left(1+\frac{Z_1}{Z_C}\right)\boldsymbol{I}_{C-C} + Z\Delta\boldsymbol{I}_{C-C}\end{aligned} \tag{10}$$

where

$$\Delta = \frac{Z_1 + Z_2 + Z_C}{Z_2 Z_C} \tag{11}$$

Making the output current $\boldsymbol{I}_{C-C}$ irrelevant to load impedance Z, it is required that $\Delta = 0$, i.e.,

$$\omega^2 = \frac{1}{L_1 C + L_2 C} \tag{12}$$

Moreover, it has a constant current output under the condition of $\Delta = 0$

$$\boldsymbol{I}_{C-C} = \frac{L_1 + L_2}{L_2}\boldsymbol{I}_{IN} \tag{13}$$

A. CV OUTPUT CHARACTERISTICS OF LCC-S COMPENSATION TOPOLOGY

When the ACSs S_1 and S_2 are both off, as shown in Fig. 3, the FHA method is utilized for analysis, and the parasitic resistances of inductance and the equivalent series resistances (ESRs) of capacitance are omitted. This is a standard LCC-S compensation topology, and the equivalent T model for the CV mode is shown in Fig. 6(a). The angular frequency of $\boldsymbol{U}_{AB}$ is defined as ω_0 and is referred to as the operation angular frequency of the resonant network hereafter. L_{IN} is made to resonate with C_P, i.e., $\omega_0^2 = 1/(L_{IN}C_P)$. According to Fig. 5(a) as well as (8), the primary coil current IP can be obtained as

$$\boldsymbol{I}_P = -j\boldsymbol{U}_{AB}\sqrt{\frac{C_P}{L_{IN}}} = -j\frac{\boldsymbol{U}_{AB}}{\omega_0 L_{IN}} \tag{14}$$

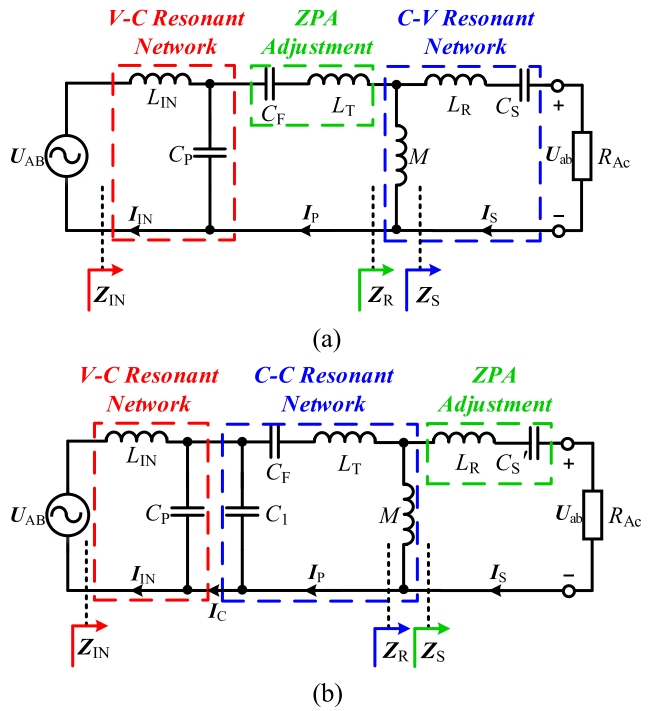

FIGURE 6. **Equivalent T models of proposed hybrid LCC-S topology (a) for CV mode; (b) for CC mode.**

Under the condition that $\boldsymbol{U}_{AB}$, L_{IN}, and ω_0 are constants, the RMS value of $\boldsymbol{I}_P$ is also a constant and is irrelevant to the other parameters of the resonant topology.

Thus, the input of the C-V resonant network shown in Fig. 6(a) can be perceived as an ACCS. In addition, when the value of C_S is sufficiently large, the series connection of L_R and C_S can be regarded as an equivalent capacitance C', i.e.,

$$C' = \frac{C_S}{1 - \omega_0^2 L_R C_S} \tag{15}$$

When M resonates with C', in combination with (6), (7), and (15), the following equation can be derived:

$$\omega_0^2 = \frac{1}{MC'} = \frac{1}{L_S C_S} \tag{16}$$

Clearly, based on the above equations, according to Fig. 5(b) as well as (9), the AC output voltage $\boldsymbol{U}_{ab}$ can be given as

$$\boldsymbol{U}_{AB} = j\omega M \boldsymbol{I}_P = \frac{M\boldsymbol{U}_{AB}}{L_{IN}} \tag{17}$$

Substituting (17) into (2), the battery charging voltage U_{Bat} in CV mode can be expressed as

$$U_{Bat} = \frac{\pi\sqrt{2}}{4} U_{AB} = \frac{\pi\sqrt{2}}{4}\frac{MU_{AB}}{L_{IN}} \tag{18}$$

where U_{ab} and U_{AB} are the RMS values of $\boldsymbol{U}_{ab}$ and $\boldsymbol{U}_{AB}$, under the condition that $\omega_0^2 = 1/(L_{IN}C_P) = 1/(L_S C_S)$, and the parameters of the compensation topology shown in Fig. 6(a) are constants. From (18), it can be seen that the battery charging voltage U_{Bat} is a constant without variable frequency and is independent of load.

On the other hand, ZPA should be implemented to lower the volt-ampere (VA) rating of the power supply [18]. According to Fig. 6(a), the secondary side equivalent impedance $\boldsymbol{Z}_S$ can be calculated as

$$\boldsymbol{Z}_S = jX + R_{Ac} \tag{19}$$

where $X = \omega_0 L_R - 1/(\omega_0 C_S)$. The reflected impedance $\boldsymbol{Z}_R$, which is converted from the secondary side to the primary side, can be given as

$$\boldsymbol{Z}_R = j\omega_0 M \parallel \boldsymbol{Z}_S = \frac{j\omega_0 M \boldsymbol{Z}_S}{j\omega_0 M + \boldsymbol{Z}_S} \tag{20}$$

where the symbol "//" represents the parallel connection of impedance. In combination with (19) and (20), the total input impedance $\boldsymbol{Z}_{IN}$ can be given as

$$\boldsymbol{Z}_{IN} = \left[\left(j\omega_0 L_T + \frac{1}{j\omega_0 C_F} + \boldsymbol{Z}_R\right) \parallel \frac{1}{j\omega_0 C_P}\right] + j\omega_0 L_{IN} \tag{21}$$

Under the condition of $\omega_0^2 = 1/(L_{IN}C_P) = 1/(L_S C_S)$, and substituting (6) into (21), $\boldsymbol{Z}_{IN}$ can be simplified as

$$\boldsymbol{Z}_{IN} = \frac{\omega_0^2 C_F L_{IN} R_{Ac}}{AR_{Ac} + \omega_0^4 M^2 C_P C_F} \tag{22}$$

where A $= j\omega_0(L_P - L_{IN}) + 1/j\omega_0 C_F$. ZPA can only be achieved under the condition that $\boldsymbol{Z}_{IN}$ presents a resistive characteristic, i.e., A $= 0$. Thus, C_F should satisfy the following equation:

$$C_F = \frac{L_{IN}C_P}{L_P - L_{IN}} \tag{23}$$

When the other parameters are fixed, C_F should be designed as per (23) to achieve ZPA. Substituting (4) into (22), the input impedance of ZPA in CV mode can be given as

$$\boldsymbol{Z}_{IN} = \frac{8}{\pi^2}\frac{L_{IN}^2 R_{Bat}}{M^2} \tag{24}$$

B. CC OUTPUT CHARACTERISTICS OF LCC-S COMPENSATION TOPOLOGY

When the ACSs S_1 and S_2 are both on, as shown in Fig. 3, a similar analysis method to that in Section II-A is used, and the equivalent T model for CC mode is shown in Fig. 6(b). If the parallel connections of capacitance on the primary and secondary sides are considered to be whole capacitances C'_P and C'_S, respectively, there are

$$\begin{cases} C'_P = C_P + C_1 \\ C'_S = C_S + C_2 \end{cases} \tag{25}$$

Comparing Fig. 6(a) and (b), the parameters of the resonant network are varied. However, both topologies are almost identical in terms of structure.

When L_{IN} resonated with C_P, i.e., $\omega_0^2 = 1/(L_{IN}C_P)$. Based on the previous analysis, it is clear that $\boldsymbol{I}_C$ is magnitude-constant, and $\boldsymbol{I}_C = -j\,U_{AB}/(\omega_0 L_{IN})$.

Similarly, the input of the C-C resonant network shown in Fig. 6(b) can be seen as an ACCS. In addition, when L_T is large enough, the series connection of L_T and C_F can be regarded as an equivalent inductance L', i.e.,

$$L' = L_T - \frac{1}{\omega_0^2 C_F} \tag{26}$$

When M resonated with C_1 and L', in combination with (6), (12) and (26), following equation can be derived as

$$\omega_0^2 = \frac{1}{L'C_1 + MC_1} = \frac{1}{L'_P C_1} \tag{27}$$

where L'_P is an equivalent inductance that includes the series connection of L_P and C_F, and $L'_P = L_P - 1/(\omega_0^2 C_F)$.

Obviously, based on the above equations, and according to (13) and Fig. 5(c), the AC output current $\boldsymbol{I}_S$ can be given as

$$\boldsymbol{I}_S = \frac{M + L'}{M}\boldsymbol{I}_C = -j\frac{\boldsymbol{U}_{AB} L'_P}{\omega_0 M L_{IN}} \tag{28}$$

Substituting (28) into (3), the battery charging current I_{Bat} in CC mode can be expressed as

$$I_{Bat} = \frac{2\sqrt{2}}{\pi} I_S = \frac{2\sqrt{2}}{\pi}\frac{U_{AB} L'_P}{\omega_0 M L_{IN}} \tag{29}$$

where I_S and U_{AB} are the RMS values of $\boldsymbol{I}_S$ and $\boldsymbol{U}_{AB}$, under the conditions that $\omega_0^2 = 1/(L_{IN}C_P) = 1/(L'_P C_1)$, and the parameters of the compensation topology as shown in Fig. 6(b) are constants. From (29), it can be seen that without variable frequency, the battery charging current I_{Bat} is constant and independent of load.

Similar to the analysis of the CV mode, ZPA should be implemented to reduce the VA rating of the power supply in the CC mode. According to Fig. 6(b), the secondary side equivalent impedance $\mathbf{Z}_S$ can be calculated as

$$\mathbf{Z}_S = jX' + R_{Ac} \tag{30}$$

where $X' = \omega_0 L_R - 1/(\omega_0 C'_S)$. The reflected impedance $\mathbf{Z}_R$, which is converted from the secondary side to the primary side, can be calculated according to (20). Thus, according to Fig. 6(b), the total input impedance $\mathbf{Z}_{IN}$ can be given as

$$\mathbf{Z}_{IN} = \left[\left(j\omega_0 L_T + \frac{1}{j\omega_0 C_F} + \mathbf{Z}_R\right) \parallel \frac{1}{j\omega_0 C_1}\right] \parallel \frac{1}{j\omega_0 C_P} + j\omega_0 L_{IN} \tag{31}$$

Under the condition of $\omega_0^2 = 1/(L_{IN}C_P) = 1/(L'_P C_1)$, and substituting (6) and (25) to (31), $\mathbf{Z}_{IN}$ can be simplified as

$$\mathbf{Z}_{IN} = \frac{\omega_0^4 M^2 L_{IN} C_1}{\omega_0^2 L_P C_P R_{Ac} + j\omega_0^2 \left(X' L_P C_P - \omega_0 M^2 C'_P\right)} \tag{32}$$

From (32), the conditional expression of the ZPA implementation can be derived as

$$X' L_P C_P - \omega_0 M^2 C'_P = 0 \tag{33}$$

Substituting (25) and "$X' = \omega_0 L_R - 1/(\omega_0 C'_S)$" into (33), the capacitance C'_S that satisfies ZPA can be deduced as follows:

$$C'_S = \frac{L'_P C_P}{\omega_0^2 \left(L'_P L_S C_P - M^2 C'_P\right)} \tag{34}$$

When the other parameters are fixed, C'_S should be designed as per (34) to achieve ZPA. Substituting (4) into (32), the input impedance of ZPA in the CC mode can be given as

$$\mathbf{Z}_{IN} = \frac{\pi^2}{8}\frac{\omega_0^2 M^2 L_{IN} C_1}{L_P C_P R_{Bat}} \tag{35}$$

C. PARAMETER MODIFICATION-BASED CC AND CV MODE IMPLEMENTATION FOR THE WPT SYSTEM

Generally, compensation topology parameters are key elements which affect the efficiency, output characteristics, and voltage/current stress of the WPT system [32]. The parameter design method for CC/CV output implementation of the proposed switching hybrid compensation topology is presented in detail below. As shown in Fig. 3, capacitances C_P and C_F, inductance L_{IN}, and an LCT are shared in both the CC and CV modes. In this study, under the condition that the LCT parameters are given, the parameters of the proposed hybrid LCC-S topology are designed as per the specified output current/voltage.

First of all, in the hybrid LCC-S topology for CV charging mode is shown in Fig. 6(a), under the condition of ZPA, the following equation can be derived from (18)

$$L_{IN} = \frac{\pi\sqrt{2}}{4}\frac{MU_{AB}}{U_{Bat}} \tag{36}$$

where U_{AB} is the RMS value of $\boldsymbol{U}_{AB}$. According to $M = k\sqrt{L_P L_S}$, and only fundamental components of $\boldsymbol{U}_{AB}$ are considered. By substituting (1) into (36), (36) can be modified as follows:

$$L_{IN} = \frac{k\sqrt{L_P L_S} U_{DC}}{U_{Bat}} \tag{37}$$

Since there is $\omega 02 = 1/(\text{LIN CP})$ in the case of ZPA, CP can be calculated as

$$C_P = \frac{1}{\omega_0^2 L_{IN}} \tag{38}$$

Under the condition that L_{IN} and C_P are determined, C_F should be calculated as per (23) for the system to operate in ZPA. According to (16), C_S can be given as

$$C_S = \frac{1}{\omega_0^2 L_S} \tag{39}$$

In the proposed switching hybrid topology, as shown in Fig. 3, the resonant network devices are shared as far as possible to reduce cost as well as volume. Hence, on the premise of constant LCT parameters, L_{IN}, C_P and C_F are shared in both the CV and CC charging modes. According to the analysis given in Section II-A, the condition for achieving ZPA is that the series equivalent impedance of L_P and C_F equals the impedance of L_{IN}, i.e., $L'_P = L_{IN}$. In combination

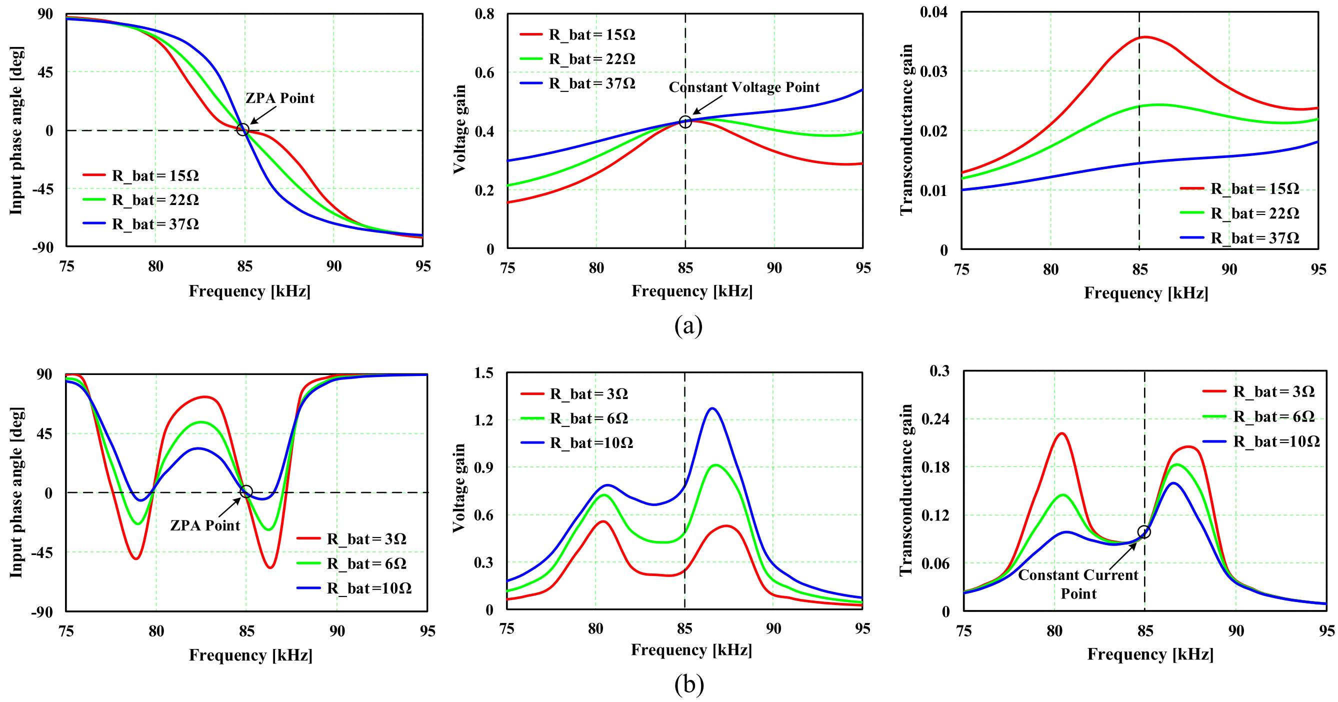

FIGURE 7. Input phase angle, voltage gain and transconductance gain of proposed hybrid LCC-S topology (a) for CV mode; (b) for CC mode.

TABLE 1. Specifications and parameters of the WPT system.

Symbol	Quantity	Symbol	Quantity
U_{DC}	300 V	L_{IN}	44.68 μH
ω_0	$(2\pi \times 85k)$ rad/s	C_P	78.54 nF
k	0.09	C_1	78.54 nF
M	19.4 μH	C_F	22.21 nF
L_P	203 μH	C_S	15.32 nF
L_S	229 μH	$C_S{}'$	16.54 nF

with (27), in the hybrid LCC-S topology for CC charging mode, as shown in Fig. 6(b), C_1 is designed as

$$C_1 = C_P \tag{40}$$

Substituting (25) and (40) to (34), C_S' can be given as

$$C_S' = \frac{L_{IN}}{\omega_0^2 \left(L_{IN} L_S - 2M^2\right)} \tag{41}$$

In this study, as per the SAE J2954 [33] recommended practice, an LCT for WPT 1 power level (3.7 kVA) is designed. In addition, under the condition that the LCT parameters are supplied, the parameters of the proposed hybrid topology are designed based on the previously introduced design methods. These parameters are shown in Table 1.

The input phase angle θ_{IN} of proposed hybrid LCC-S topology is defined as

$$\theta_{IN} = \frac{180^\circ}{\pi} \tan^{-1} \frac{\mathrm{Im}\,(Z_{IN})}{\mathrm{Re}\,(Z_{IN})} \tag{42}$$

where the operators "Im" and "Re" represent the imaginary and real parts, respectively, of the input impedance. The voltage gain G_V and transconductance gain G_T of LCC-S compensation topology are defined as follows:

$$G_V = \frac{U_{ab}}{U_{AB}} = \frac{U_{Bat}}{U_{DC}} \tag{43}$$

$$G_T = \frac{I_{Bat}}{U_{AB}} = \frac{I_S}{U_{DC}} \tag{44}$$

In order to theoretically verify the previous analyses, PSIM simulation is carried out with the parameters as shown in Table 1; the simulation results are shown in Fig. 7. The ZPA could be achieved at designed resonant frequency (85 kHz) in both the CC and CV modes. In addition, the output voltage in CV mode and output current of CC mode are both constants at 85 kHz.

In the proposed switching hybrid LCC-S WPT system shown in Fig. 3, the CC and CV modes are intelligently selected based on the battery charging voltage and current by controlling the two ACSs (S_1,S_2). Generally, ACSs can be implemented by two series-opposing connected MOSFETs or two anti-paralleled insulated-gate bipolar transistors (IGBTs). The MOSFET-type ACSs are utilized in this study, and the control logic for S_1 and S_2 is shown in Fig. 8.

The WPT system control flowchart is shown in Fig. 9. After the WPT system initialization and start, the battery charging voltage U_{Bat} and current I_{Bat} are synchronously acquired via voltage and current sensors and sent to the secondary controller. U_{Spe} is the specified battery charging voltage in CV mode, i.e., the critical voltage of the

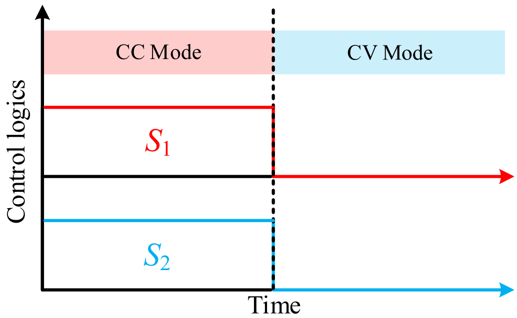

FIGURE 8. Control logic for S_1 and S_2 of switching hybrid WPT system.

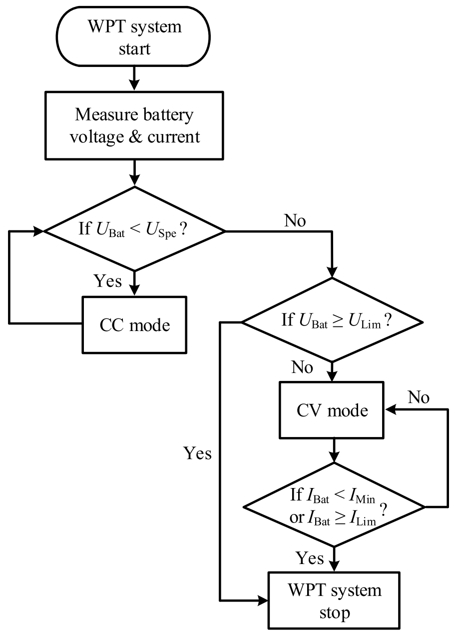

FIGURE 9. Control flowchart of the proposed WPT system for CC/CV charging.

conversion point between the CC and CV modes. When the secondary controller senses that U_{Bat} is lower than U_{Spe}, the CC mode is selected, and the secondary controller drives S_2 to the "ON" state. Meanwhile, the secondary controller sends a state conversion request to the primary controller via Bluetooth. After receiving the signal, the primary controller drives S_1 to the "ON" state, and synchronously begins to drive the four MOSFETs (Q_1–Q_4) of the FBI with 0.5 duty cycle pulse-width modulation (PWM) signals. In the proposed hybrid LCC-S WPT system, symmetrical control with constant frequency is applied.

However, when the secondary controller senses that U_{Bat} is higher than or equal to U_{Spe}, the CV mode is selected. Similar to the previously described control process, S_1 and S_2 are driven to an "OFF" state by the primary and secondary controllers, respectively. In the control flowchart shown in Fig. 8, I_{Min} is the specified lower limit of the charging current. In the final stage of the CV mode, if the secondary controller senses that I_{Bat} is lower than I_{Min}, charging will be terminated. In addition, U_{Lim} and I_{Lim} are the specified ceiling voltage

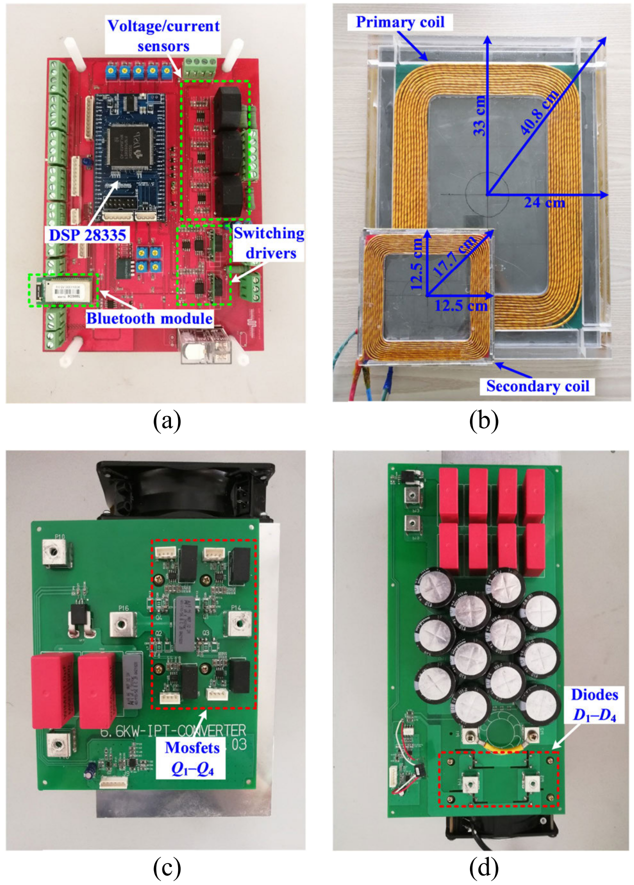

FIGURE 10. Experimental setup. (a) DSP 28335 controller. (b) Transmitting and receiving coils. (c) FBI. (d) Rectifier.

and current of the battery. Whenever the charging voltage or current is higher than the upper limit value, charging will also be stopped. All the control signals (charging start/stop, state conversion, etc.) are transmitted from the secondary side to the primary side via Bluetooth.

III. EXPERIMENTAL VERIFICATION

In order to verify the previous analyses and designs, a 2.5-kW experimental WPT prototype is configured. The major components of the prototype are shown in Fig. 10. Two identical control boards are arranged on the primary and secondary sides, respectively. As shown in Fig. 10(a), the TMS320F28335 DSP, voltage/current sensors, switching drivers and Bluetooth module are integrated. Fig. 10(b) shows a pair of coupling coils, which are manufactured based on the WPT1 level of the SAE J2954 recommended practice. Because of the manufacturing deviations, the practical parameters of transmitting coil are L_P: 203.8 μH, Length: 580 mm, Width: 430 mm, and of receiving coil are L_S: 228.1 μH, Length × Width: 250 mm × 250 mm, respectively. The thickness of the airgap between the primary and secondary coil is 15 cm. Litz wires (primary coil: AWG 9, secondary coil: AWG 13) are utilized to curtail skin and proximity effects. Both primary and secondary

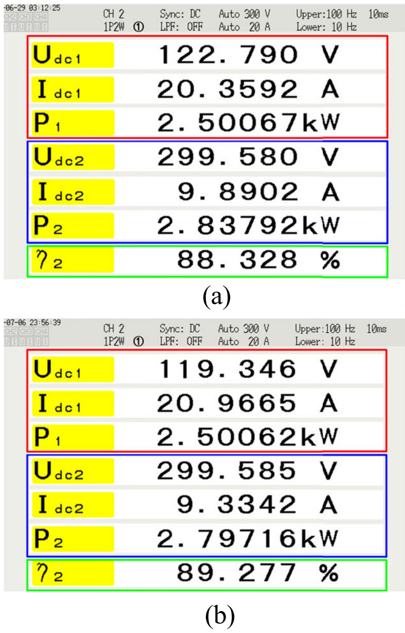

FIGURE 11. Experimental results of the critical charge point between CC and CV modes. (U_{dc1}, I_{dc1}, and P_1 are the battery charging voltage, current and power, respectively; U_{dc2}, I_{dc2}, and P_2 are the DC-link voltage, input DC current and power, respectively; η_2 is the DC efficiency). (a) In CV mode; (b) In CC mode.

magnetic pads (80 mm thickness) consisted of PC95 ferrite, and four MOSFETs (C3M0030090K) and four diodes (IDW20G120C5B) are selected to construct the FBI and rectifier, respectively.

The proposed LCC-S hybrid topology is configured according to the parameters listed in Table 1. The parameters are measured with an LCR meter (HIOKI IM3536), and the deviation between the designed parameters and practical parameters is found to be less than 1%. Comparative experiments between the CC and CV modes are carried out using the parameters and experimental prototype. As shown in Fig. 7, ZVS can be achieved in both the CC and CV modes when the switching frequency is slightly lower than the ZPA frequency. Thus, throughout the charging process, the practical switching frequency is set to f0 = 84.8 kHz and kept constant. In this study, the DC-link voltage U_{DC} is supplied by an DC power source (LAB-DSP 350-08.4), and the available load is a battery array consisting of four 24 V lithium batteries connected in series. Based on these laboratorial limitations, U_{DC} is selected as 300 V, and the specified values of I_{Bat} and U_{Bat} are designed to 21.5 A and 120V, respectively. In addition, the maximum efficiency and charge power are designed to be obtained from the critical charge point between the CC and CV modes. The charge parameters are measured using a power analyzer (HIOKI PW6001), and the measured results of the critical charge point are shown in Fig. 11. The DC outputs and inputs are shown in the red and blue frames, respectively, and the DC efficiency is displayed in the green frame. At the critical charge point, the charge powers of both the CC and CV modes

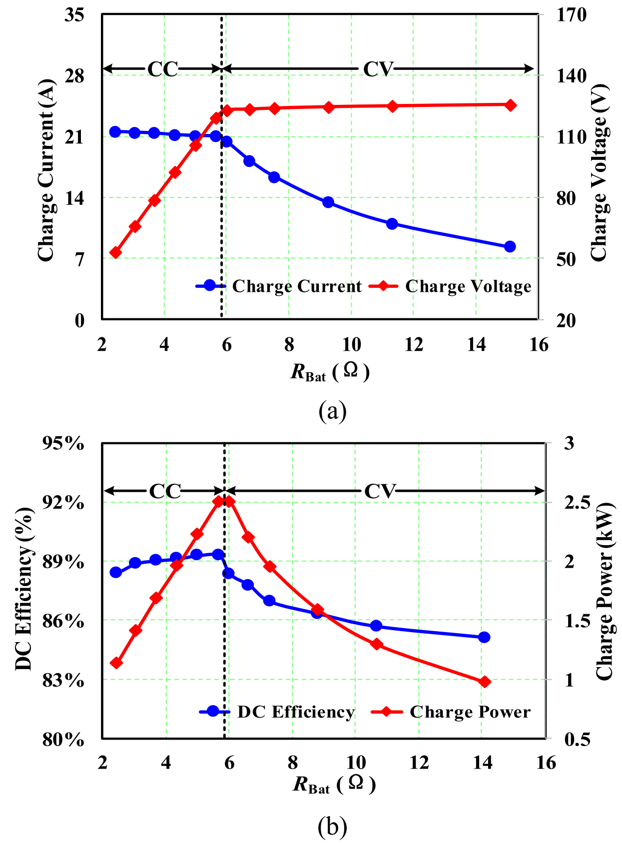

FIGURE 12. Charging characteristics of the proposed hybrid charger. (a) Measured charging profile; (b) Measured DC efficiency and charging power.

are almost 2.5 kW, and their DC efficiencies are 89.28 % and 88.33%, respectively. The charging characteristics of the proposed hybrid charger are shown in Fig. 12; it can be observed that during continuous charging, the battery equivalent resistance R_{Bat} increases from 2.458 Ω to 5.69 Ω in CC mode, and 6.03 Ω to 14.12 Ω in CV mode. In Fig.12(a), it can be observed that as R_{Bat} increases, the charge current (21.53 A–20.97 A) in CC mode and charge voltage (122.79 V–125.97 V) in CV mode are almost constants. The slight deviations in the current and voltage in CC mode and CV mode, respectively, are mainly caused by parasitic impedances, parameter errors and ZPA point deviations. In addition, in the coil manufacturing process, although Lize wires are utilized to curtail skin and proximity effects, the equivalent series resistance (ESR) of the coils is hard to completely eliminate. All of these factors may slightly affect the outputs. Measured DC efficiency and charge power are shown in Fig. 12(b); as the R_{Bat} increases, both DC efficiency and charge power increase in CC mode and decrease in CV mode. The maximum DC efficiency (89.28%) and charge power (2500.7 W) are observed at the charge critical point ($R_{Bat} = 5.69\Omega$).

The experimental waveforms are captured using an oscilloscope (Teledyne LeCroy HDO4034A). Under the condition of load fluctuations, the observations are shown in Fig. 13.

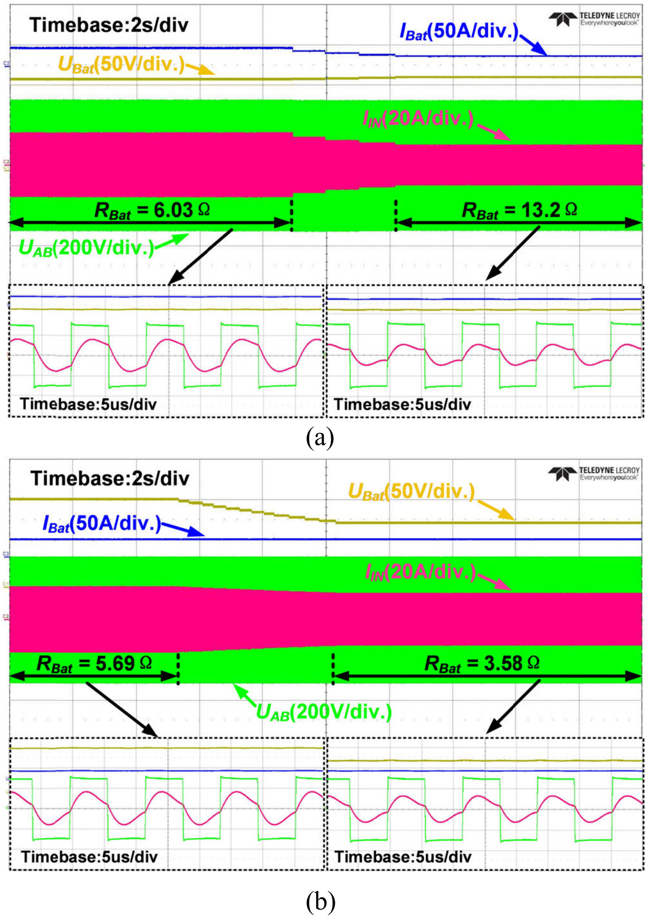

FIGURE 13. Experimental waveforms of U_{Bat}, I_{Bat}, U_{AB}, and I_{IN} with load fluctuations. (a) In CV mode, and R_{Bat} varies from 6.03Ω to 13.2Ω; (b) In CC mode, and R_{Bat} varies from 5.69 Ω to 3.58 Ω.

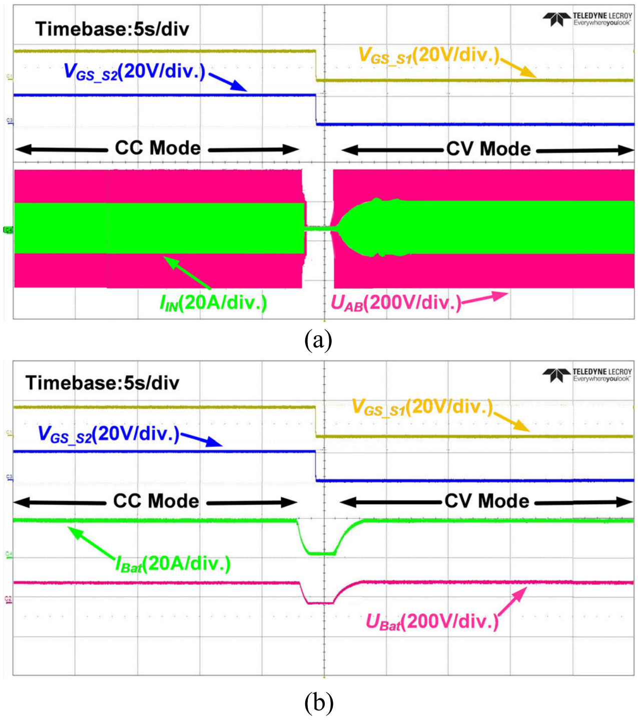

FIGURE 14. Transient waveforms from CC mode to CV mode, and V_{GS_S1} and V_{GS_S2} are the gate drive signals of two ACSs (S_1 and S2). (a) The waveforms of input AC voltage U_{AB} and input AC current I_{IN}. (b) the waveforms of battery charging voltage U_{Bat} and charging current I_{Bat}.

In CV mode, when the R_{Bat} fluctuated from 6.03 Ω to 13.2 Ω, the charge voltage U_{Bat} is nearly unchanged, and charge current IBat and AC input current I_{IN} decreased continuously. On the contrary, in CC mode, as shown in Fig. 13(b), the charge current I_{Bat} is almost constant when the R_{Bat} fluctuated from 5.69 Ω to 3.58 Ω, and U_{Bat} and $\boldsymbol{I}_{\text{IN}}$ decreased continuously. In both CC and CV modes, ZVS is achieved within a minor input phase angle. In addition, the transient experiments are also carried out. The transient waveforms at the conversion point from CC mode to CV mode are shown in Fig. 14. Considering the possible problems caused by the transition point, e.g., high current/voltage spikes and the chaos of ZVS, a switching method is proposed here to avoid the problems. A short period of time before and after the mode convention point, the four PWM signals of the FBI are closed briefly. In this way, even though it causes a short charging pause, for a few hours of charging process, this effect can be ignored. In Fig. 14(a), the U_{AB} remain unchanged both in CC and CV modes, and the value of I_{IN} in CC mode is slightly smaller than the value in CV mode. The transient waveforms of battery charging voltage U_{Bat} and charging current I_{Bat} are shown in Fig. 14(b). Both of them are nearly constant during the transient process. The plausibility of the proposed LCC-S hybrid charger is verified via the above experimental results.

IV. CONCLUSION

In this study, a switching hybrid compensation topology for EV wireless charging is proposed. Two additional capacitors are added to an LCC-S topology and controlled via two ACSs for CC and CV charging. The CC, CV and ZPA characteristics could be implemented with ease using the proposed topology. The identical LCT, compensation inductor and capacitor are shared between CC and CV charging modes; in addition, the operation frequency remained unchanged throughout the charging process. The specific characteristics of the proposed hybrid topology are theoretical analyzed via the T model of LCT. The topology parameter design procedures are plainly specified as per the given CC and CV. Based on the weak communication between the transmitter and receiver, the control flows of the proposed hybrid system are introduced, and a 2.5-kW experimental prototype is configured to verify the charging performances of the proposed hybrid charger. The experimental results show that the practically obtained CC and CV values of the proposed topology are very close to the designed values. The maximum DC efficiency (89.28%) and charge power (2500.7 W) are achieved at the critical charge point. The charging characteristics also remained stable during load fluctuation.

REFERENCES

[1] S. Li and C. C. Mi, "Wireless power transfer for electric vehicle applications," *IEEE J. Emerg. Sel. Topics Power Electron.*, vol. 3, no. 1, pp. 4–17, Mar. 2015.

[2] Y. Jang and M. M. Jovanovic, "A contactless electrical energy transmission system for portable-telephone battery chargers," *IEEE Trans. Ind. Electron.*, vol. 50, no. 3, pp. 520–527, Jun. 2003.

[3] S. Y. R. Hui and W. W. C. Ho, "A new generation of universal contactless battery charging platform for portable consumer electronic equipment," *IEEE Trans. Power Electron.*, vol. 20, no. 3, pp. 620–627, May 2005.

[4] C. Bil, M. Simic, and V. Vojisavljevic, "Design of a recharge station for UAVS using non-contact wireless power transfer," in *Proc. 54th AIAA Aerosp. Sci. Meeting*, Jan. 2016, p. 1525.

[5] S. Liu, Z. Ye, and W. Lu, "Electric vehicle dynamic wireless charging technology based on multi-parallel primary coils," in *Proc. IEEE Int. Conf. Electron. Commun. Eng. (ICECE)*, Dec. 2018, pp. 120–124.

[6] C.-G. Kim, D.-H. Seo, J.-S. You, J.-H. Park, and B. H. Cho, "Design of a contactless battery charger for cellular phone," *IEEE Trans. Ind. Electron.*, vol. 48, no. 6, pp. 1238–1247, Dec. 2001.

[7] Z. Wang, X. Lai, and Q. Wu, "A PSR CC/CV flyback converter with accurate cc control and optimized CV regulation strategy," *IEEE Trans. Power Electron.*, vol. 32, no. 9, pp. 7045–7055, Sep. 2017.

[8] V.-L. Tran, H.-N. Vu, D.-D. Tran, and W. Choi, "Design and implementation of a high-efficiency multiple output charger based on the time-division multiple control technique," *IEEE Trans. Power Electron.*, vol. 32, no. 2, pp. 1210–1219, Feb. 2017.

[9] H.-N. Vu and W. Choi, "A novel dual full-bridge LLC resonant converter for CC and CV charges of batteries for electric vehicles," *IEEE Trans. Ind. Electron.*, vol. 65, no. 3, pp. 2212–2225, Mar. 2018.

[10] Y. Li, J. Hu, F. Chen, S. Liu, Y. Zhaotian, and Z. He, "A new-variable-coil-structure-based IPT system with load-independent constant output current or voltage for charging electric bicycles," *IEEE Trans. Power Electron.*, vol. 33, no. 10, pp. 8226–8230, Oct. 2018.

[11] M. Pahlevaninezhad, D. Hamza, and P. K. Jain, "An improved layout strategy for common-mode EMI suppression applicable to high-frequency planar transformers in high-power DC/DC converters used for electric vehicles," *IEEE Trans. Power. Electron.*, vol. 29, no. 3, pp. 1211–1228, Mar. 2014.

[12] K. Na, H. Ma, G. Namgoon, and K. Kim, "Step-charging technique for CC/CV mode battery charging with low-cost control components in IPT systems," *IEEE Power. Electron.*, vol. 11, no. 15, pp. 2523–2530, Dec. 2018.

[13] D. Ahn, S. Kim, J. Moon, and I.-K. Cho, "Wireless power transfer with automatic feedback control of load resistance transformation," *IEEE Trans. Power Electron.*, vol. 31, no. 11, pp. 7876–7886, Nov. 2016.

[14] H. Li, J. Li, K. Wang, W. Chen, and X. Yang, "A maximum efficiency point tracking control scheme for wireless power transfer systems using magnetic resonant coupling," *IEEE Trans. Power Electron.*, vol. 30, no. 7, pp. 3998–4008, Jul. 2015.

[15] D. Ahn and S. Hong, "Wireless power transfer resonance coupling amplification by load-modulation switching controller," *IEEE Trans. Ind. Electron.*, vol. 62, no. 2, pp. 898–909, Feb. 2015.

[16] J. Byeon, M. Kang, M. Kim, D.-M. Joo, and B. K. Lee, "Hybrid control of inductive power transfer charger for electric vehicles using LCCL-S resonant network in limited operating frequency range," in *Proc. IEEE ECCE*, Sep. 2018, pp. 1–6.

[17] X. Ren, Q. Chen, L. Cao, X. Ruan, S.-C. Wong, and C. K. Tse, "Characterization and control of self-oscillating contactless resonant converter with fixed voltage gain," in *Proc. IEEE ECCE*, Jun. 2012, pp. 1822–1827.

[18] W. Zhang and C. C. Mi, "Compensation topologies for high power wireless power transfer systems," *IEEE Trans. Veh. Technol.*, vol. 65, no. 6, pp. 4768–4778, Jun. 2016.

[19] C. Auvigne, P. Germano, D. Ladas, and Y. Perriard, "A dual-topology ICPT applied to an electric vehicle battery charger," in *Proc. 20th Int. Conf. Elect. Mach.*, Sep. 2012, pp. 2287–2292.

[20] X. Qu, H. Han, S.-C. Wong, C. K. Tse, and W. Chen, "Hybrid IPT topologies with constant current or constant voltage output for battery charging applications," *IEEE Trans. Power Electron.*, vol. 30, no. 11, pp. 6329–6337, Nov. 2015.

[21] R. Mai, Y. Chen, Y. Li, Y. Zhang, G. Cao, and Z. He, "Inductive power transfer for massive electric bicycles charging based on hybrid topology switching with a single inverter," *IEEE Trans. Power Electron.*, vol. 32, no. 8, pp. 5897–5906, Aug. 2017.

[22] Y. Chen, Z. Kou, Y. Zhang, Z. He, R. Mai, and G. Cao, "Hybrid topology with configurable charge current and charge voltage output-based WPT charger for massive electric bicycles," *IEEE J. Emerg. Sel. Topics Power Electron.*, vol. 6, no. 3, pp. 1581–1594, Sep. 2018.

[23] Y. Chen, B. Yang, Z. Kou, Z. He, G. Cao, and R. Mai, "Hybrid and reconfigurable IPT systems with high-misalignment tolerance for constant-current and constant-voltage battery charging," *IEEE Trans. Power Electron.*, vol. 33, no. 10, pp. 8259–8269, Oct. 2018.

[24] Z. Li, K. Song, G. Wei, J. Jiang, and C. Zhu, "A 3-kW wireless power transfer system for sightseeing car supercapacitor charge," *IEEE Trans. Power Electron.*, vol. 32, no. 5, pp. 3301–3316, May 2016.

[25] K. Song, Z. Li, J. Jiang, and C. Zhu, "Constant current/voltage charging operation for series-series and series-parallel compensated wireless power transfer systems employing primary-side controller," *IEEE Trans. Power Electron.*, vol. 33, no. 9, pp. 8065–8080, Sep. 2018.

[26] Z. Li, G. Wei, S. Dong, K. Song, and C, Zhu, "Constant current/voltage charging for the inductor-capacitor-inductor-series compensated wireless power transfer systems using primary-side electrical information," *IET Power Electron.*, vol. 11, no. 14, pp. 2302–2310, Nov. 2018.

[27] R. Mai, R. Dai, Z. Zhu, Mingxuan Li, Y. Chen, W. Li, and Z. He, "Optimization of time-weighted average efficiency for reconfigurable IPT battery charging system," *IEEE Access*, vol. 7, pp. 43092–43099, 2019.

[28] F. Liu, K. Chen, Z. Zhao, K. Li, and L. Yuan, "Transmitter-side control of both the CC and CV modes for the wireless EV charging system with the weak communication," *IEEE J. Emerg. Sel. Topics Power Electron.*, vol. 6, no. 2, pp. 4401–4409, Oct. 2017.

[29] J. L. F. Vieira, J. A. Oliver, P. Alou, and J. A. Cobos, "Power converter topologies for a high performance transformer rectifier unit in aircraft applications," in *Proc. 11th IEEE/IAS Int. Conf. Ind. Appl.*, Dec. 2014, pp. 1–8.

[30] R. L. Steigerwald, "A comparison of half-bridge resonant converter topologies," *IEEE Trans. Power Electron.*, vol. PEL-3, no. 2, pp. 174–182, Apr. 1988.

[31] Z. Cheng, L. Yang, S. Kai, and C. Zhu, "Design and loss analysis of loosely coupled transformer for an underwater high-power inductive power transfer system," *IEEE Trans. Magn.*, vol. 51, no. 7, Jul. 2015, Art. no. 8106307.

[32] Y. Chen, H. Zhang, S.-J. Park, and D.-H. Kim, "A comparative study of S-S and LCCL-S compensation topologies in inductive power transfer systems for electric vehicles," *Energies*, vol. 12, no. 10, p. 1913, May 2019.

[33] *Wireless Power Transfer for Light-Duty Plug-In/Electric Vehicles and Alignment Methodology*. document SAE TIR J2954, May 2016.

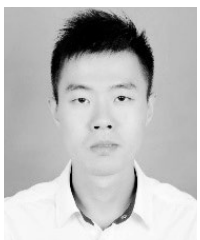

YAFEI CHEN (S'18) received the B.S. degree in electronic information engineering from Southwest Jiaotong University, Chengdu, China, in 2012, and the M.S. degree in control theory and control engineering from the Qingdao University of Science and Technology, Qingdao, China, in 2016. He is currently pursuing the Ph.D. degree in electrical engineering with Chonnam National University, Gwangju, South Korea. His research interests include power conditioning system dc–dc converters for renewable energy, battery chargers for hybrid electric vehicles (HEVs)/EVs, and wireless power transfer for EVs and unmanned aerial vehicles (UAVs).

HAILONG ZHANG (S'18) received the B.S. degree in electronic engineering and automation from China Petroleum University, Dongying, China, in 2013, and the M.S. degree in control theory and control engineering from the Qingdao University of Science and Technology, Qingdao, China, in 2016. He is currently pursuing the Ph.D. degree in electrical engineering with Chonnam National University, Gwangju, South Korea. His research interests include wireless power transfer system for UAVs, power conversion system for EVs, and renewable energy storage systems.

SUNG-JUN PARK received the B.S., M.S., and Ph.D. degrees in electrical engineering, and the Ph.D. degree in mechanical engineering from Pusan National University, Busan, South Korea, in 1991, 1993, 1996, and 2002, respectively. From 1996 to 2000, he was an Assistant Professor with the Department of Electrical Engineering, Koje College, Koje, South Korea. From 2000 to 2003, he was an Assistant Professor with the Department of Electrical Engineering, Tong-Myong College, Busan. Since 2003, he has been a Professor with the Department of Electrical Engineering, Chonnam National University, Gwangju, South Korea. His research interests include power electronics, motor control, mechatronics, and micromachine automation.

DONG-HEE KIM (S'10–M'15) received the B.S., M.S., and Ph.D. degrees from Sungkyunkwan University, Suwon, South Korea, in 2009, 2011, and 2015, respectively, all in electrical engineering.

From 2015 to 2016, he was a Postdoctoral Researcher with Sunkyunkwan University. Since 2016, he has been a part-time Lecturer with Daejin University, Pocheon, South Korea, and the Shandong University of Technology, Shandong, China, respectively. From September 2016 to August 2017, he was an Assistant Professor with Tongmyong University, Busan, South Korea. In September 2017, he joined Chonnam National University, Gwangju, South Korea, as an Assistant Professor. His research interests include power conditioning system dc–dc converters for renewable energy, battery chargers for hybrid electric vehicles/electric vehicles, and wireless power transfer for EVs and UAVs.